Title

Longitudinal Imaging and Analysis of Neurons Expressing Polyglutamine-Expanded Proteins

Authors

Tsvetkov, Andrey S
Ando, D Michael
Finkbeiner, Steven

Publication Date

2013

DOI

10.1007/978-1-62703-438-8_1

Peer reviewed

Chapter 1

Longitudinal Imaging and Analysis of Neurons Expressing Polyglutamine-Expanded Proteins

Andrey S. Tsvetkov, D. Michael Ando, and Steven Finkbeiner

Abstract

Misfolded proteins have been implicated in most of the major neurodegenerative diseases, and identifying drugs and pathways that protect neurons from the toxicity of misfolded proteins is of paramount importance. We invented a form of automated imaging and analysis called robotic microscopy that is well suited to the study of neurodegeneration. It enables the monitoring of large cohorts of individual neurons over their lifetimes as they undergo neurodegeneration. With automated analysis, multiple endpoints in neurons can be measured, including survival. Statistical approaches, typically reserved for engineering and clinical medicine, can be applied to these data in an unbiased fashion to discover whether factors contribute positively or negatively to neuronal fate and to quantify the importance of their contribution. Ultimately, multivariate dynamic models can be constructed from these data, which can provide a systems-level understanding of the neurodegenerative disease process and guide the rationale for the development of therapies.

Key words Huntington's disease, Neurodegeneration, Huntingtin, Survival analysis, High-throughput screening

1 Introduction

Huntington's disease (HD) is the most common inherited neurodegenerative disorder and is characterized by abnormal motor movements and cognitive decline. A polyglutamine expansion in the huntingtin (htt) protein, which causes the disease, leads to inclusion body (IB) formation and neuronal toxicity.

Studying the cellular and molecular mechanisms of HD in animal models has limitations. Phenotypes vary among the mouse models. Pharmacological or genetic manipulations in mice can be challenging and expensive. Drugs may have effects outside the CNS that confound the interpretation of results. The development of faithful cellular models of neurodegenerative disease is therefore critical to rigorously elucidate disease mechanisms, discover therapeutic targets, and identify potential therapies.

Danny M. Hatters and Anthony J. Hannan (eds.), *Tandem Repeats in Genes, Proteins, and Disease: Methods and Protocols*, Methods in Molecular Biology, vol. 1017, DOI 10.1007/978-1-62703-438-8_1,

Many cell models of HD are based on immortalized cell lines, primary murine cultures of neurons and glia, and cultured human neurons and glia differentiated from patient-derived induced pluripotent stem (iPS) cells. The main advantage of cell line-based models is their homogeneity and ease of use. However, the cellular physiology of immortalized cell lines differs in important respects from primary post-mitotic neurons, namely, in their capacity to divide and lack of synapses. Therefore, to identify mechanisms and therapeutic targets, primary neurons are likely to be a more relevant system [1–4]. The recent development of human-cell models of HD from patient-derived iPS cells should yield insights into the disease that have increased physiological relevance. This could be especially important if a major reason for the failure of clinical trials for HD therapies is because murine models of HD are not representative of the human condition [5].

In our laboratory, we use several HD models that are based on human neurons or primary murine neurons from the striatum as well as other brain regions less affected in HD [1, 5]. Cultured neurons are transfected with N-terminal fragments of wild-type (WT) or polyQ-expanded huntingtin (htt) (171, 480, 586 N-terminal amino acids or full-length htt) fused to the N-terminus of a fluorescent protein. These HD models recapitulate at least 18 molecular and cellular features observed in HD patients [2]. Moreover, with these HD neuron models, we predicted results that were later confirmed by observations in mouse models or HD patients, making these models highly physiologically relevant [6–13]. Recently, we developed a human neuron model of HD, based on iPS cells, which holds great potential for future HD research [5].

Conventional methods aimed at determining the prognostic significance of histological changes seen in fixed cultures or brain tissue have significant shortcomings. These methods rely on static histological "snapshots," in which only a fraction of neurons that degenerate are caught, while others have not yet begun to die or are degenerated (and consequently missed) completely. Therefore, inferences of cause-and-effect relationships from a time series of these snapshots can be incomplete and potentially misleading.

To overcome these limitations, we built an automated imaging system that can perform high-throughput longitudinal single-cell analysis [3, 14]. In our third-generation system, image acquisition is controlled by custom-built computer software and begins when a program instructs a robotic arm to load a plate of cells on the microscope stage. The computer instructs the microscope to focus itself and executes an algorithm that enables the microscope to position the plate in precise alignment to a reference position. The microscope then moves the plate to the center of the first well and collects fluorescence images at predetermined wavelengths, thereafter moving the stage to each adjacent field in a well. These steps are repeated until an entire well or a plate is imaged. The robotic

arm then removes the plate and puts it back in the incubator until the plate is scheduled to be imaged again.

Custom programs then analyze the images and quantify features of interest off-line. First, the program organizes the images by well, plate, and date. Each image from the same well is then electronically "stitched" together into a montage. Montages from the same well are organized by date, and the program performs a further fine alignment on the stack of montages. The analysis program then identifies each neuron from the first montage, assigning it a unique identifying number, and then tracks that cell through the subsequent montages. Thus, we can follow a large group of neurons (thousands) over time, as neurodegeneration unfolds, and identify the changes (e.g., levels of diffuse htt, IB formation) in each neuron and link these changes to some future fate of this particular neuron (survival or death), establishing cause-and-effect relationships [2, 3, 14–16].

Such datasets—composed of repeated measures on individual members of a cohort—are amenable to a powerful suite of statistical tools called survival analysis. Despite its name, this tool can be used to measure differences in essentially any time-dependent event among cohorts, including survival, and has been used widely in engineering and medicine. A related statistical tool, the Cox proportional hazards (CPH) analysis, makes it possible to construct explanatory statistical models that delineate the factors that contribute positively or negatively to a particular fate for individuals in the cohort and quantifies their relative importance. This capability is likely to be critical for studies of neurodegenerative processes, which appear to be complex, highly intertwined, and dynamic. Indeed, we found that the performance of our robotic microscope system for hypothesis-driven and discovery research is extraordinary. Direct comparisons with conventional snapshot approaches revealed that robotic microscopy is about 100- to 1,000-fold more sensitive for detecting differences in responses or behavior between cohorts. As few as eight cells per well can be sufficient to predict the complete-well result with 90 % accuracy. These advantages suggest that the robotic microscope is a uniquely powerful tool to study precious or difficult-to-culture cells (e.g., iPS cells) and for performing high-throughput screens on primary cells.

The utility and power of the approach can be illustrated with some recent applications. Using this automated imaging platform, we discovered that mutant htt-forming IBs, rather than being a toxic species themselves, were in fact a coping response used by neurons to mitigate mutant htt. Neurons that had them survived longer [14]. In a separate study, we discovered that, even before IBs form, the ubiquitin-proteasome system (UPS) becomes overwhelmed in the presence of mutant htt. Interestingly, IB formation and the accompanying sequestration of mutant htt into an IB appear to restore protein homeostasis and clearance systems [15],

offering an explanation for how IBs might help neurons to cope with mutant htt. Since IBs form asynchronously in only a subset of neurons with mutant htt, the relationship between IB formation and UPS function could only be elucidated by an approach that utilizes longitudinal single-cell analysis. Indeed, with our findings in mind, others reexamined the relationship of the UPS to IB formation in vivo and found a similar result [17].

Autophagy is a cellular mechanism that directs proteins to lysosomes for degradation and recycling and also turns over monomeric, misfolded proteins and protein aggregates. By observing striatal neurons transfected with mutant htt over time, we identified small-molecule autophagy inducers that lower the levels of mutant htt [4]. When we treated a cohort of neurons with this small-molecule autophagy inducer, we found that the levels of diffuse mutant htt dropped and, importantly, the survival of striatal neurons increased. We also observed that neurons produced fewer IBs, suggesting that the autophagy stimulator enhanced mutant htt degradation, thereby reducing the need for IBs to form as a coping response. These findings underscore how analyzing spatiotemporal changes in neurons with automated microscopy represents an unprecedented opportunity to study the mechanisms of neurodegeneration.

Although the sophistication of our third-generation robotic microscope—a product of many years of technology development and refinement—would be difficult to replicate, the basic power of longitudinal single-cell analysis can be achieved by most labs with lower-throughput manual approaches. In this chapter, we describe many of our methods and offer suggestions for how experiments similar in design and scope can be performed with simpler instrumentation.

2 Materials

2.1 Fluorescently Tagged Proteins

We co-transfect neurons with a fluorescently tagged N-terminal fragment of htt (WT or mutant) and a morphology/viability fluorescent marker. In some experiments, we perform a triple transfection by adding a third fluorophore [15].

2.1.1 An N-Terminal Fragment of htt Fused to the N-Terminus of a Fluorescent Protein

1. pGW1-CMV plasmid (British Biotechnology; Oxford, UK) that gives us the highest expression levels in striatal neurons encoding WT or mutant htt fused to GFP (*see* **Notes 1** and **2**).
2. QIAGEN plasmid isolation MAXI kit (QIAGEN; Valencia, CA). Purified plasmid is stored at 4 °C.

2.1.2 A Fluorescent Morphology and Viability Marker

1. pGW1-CMV plasmid (British Biotechnology) encoding a red fluorescent protein (*see* **Notes 3** and **4**) [14].
2. Plasmid purified with the QIAGEN plasmid isolation MAXI kit (stored at 4 °C).

2.2 Preparation of Neuronal Cultures

1. Poly-D-lysine solution (catalog number A-003-E, 1 mg/ml, Millipore; Billerica, MA).
2. Mouse laminin (catalog number 354232, 1 mg, BD Biosciences; San Jose, CA).
3. Plates: 96-well plate (catalog number 92696, Swiss TPP; Trasadingen, Switzerland) or 24-well plate (catalog number 3337, Corning) (*see* **Note 5**).
4. Trypsin inhibitor (catalog number T9253-5 G, Sigma, St. Louis, MO).
5. Papain (PAP 100 mg, Worthington; Lakewood, NJ).
6. L-Cysteine.
7. 10× KY stock solution: 10 mM kynurenic acid, 0.0025 % (w/v) phenol red (catalog number P-0290, Sigma), 5 mM HEPES, 100 mM $MgCl_2$, pH 7.4. Filter-sterilized and stored at 4 °C.
8. Dissociation medium (DM): 81.8 mM Na_2SO_4, 30 mM K_2SO_4, 5.8 mM $MgCl_2$, 0.25 mM $CaCl_2$, 1 mM HEPES, 20 mM glucose, 0.001 % (w/v) phenol red, 0.16 mM NaOH. Filter-sterilized and stored at 4 °C.
9. Opti-MEM-glucose: 4 ml of 2.5 M glucose per 500 ml of Opti-MEM (catalog number 31985, GIBCO).
10. Trypan blue.
11. For plating onto a 96-well plate: a 50-ml reservoir (catalog number 4870, Corning), a multichannel 250-µl pipettor and required tips.
12. Neurobasal medium (catalog number 21103, GIBCO).
13. 50× B27 vitamin supplement (catalog number 17504-044, GIBCO).
14. 100× GlutaMAX.
15. 100× pen/strep.
16. Dissection microscope (catalog number NI-MA-MMD31000, Nikon).
17. Tools: 2–3 pairs of forceps, one pair of scissors, a chemical spatula (catalog number 11295-10, 14060-09, 10099-15, Fine Science Tools).
18. 0.20-µm filters.
19. 30-ml syringes.
20. Cell-culture facilities including a humidified 37 °C incubator with 5 % (v/v) atmospheric CO_2, hemocytometer, and 37 °C water bath.
21. Alcohol solutions: 70 % (v/v) ethanol and 96 % (v/v) ethanol.
22. Source of primary neurons: timed-pregnant rat (or a mouse).

2.3 Transfection

1. Lipofectamine 2000 (catalog number 11668-027, Invitrogen) (*see* **Note 6**).
2. Transfection solution: 1× KY in neurobasal medium (catalog number 21103, GIBCO).
3. Opti-MEM (catalog number 31985, GIBCO).
4. Neurobasal medium (catalog number 21103, GIBCO).

2.4 Automated Microscopy

1. Digital images are obtained with an inverted microscope (a Nikon TE2000E-PFS microscope, a long-working-distance Nikon CFI S Plan Fluor 20× (NA 0.45) objective) and a 300 W Xenon Lambda LS illuminator (Sutter Instruments, Novato, CA) (*see* **Note 7**).
2. Stage movements to an adjacent well and focusing are performed with an MS-2000 XY stage (Applied Scientific Instrumentation, Eugene, OR).
3. Images are acquired with a CCD camera (Clara, Andor; Belfast, Northern Ireland) driven by Image-Pro Plus software (Media Cybernetics; Bethesda, MD).
4. Image-Pro Plus software (Media Cybernetics).

2.5 Image Analysis and Storage

1. StatView (Apple, Cupertino, CA).
2. Image J (rsbweb.nih.gov/ij/, the National Institutes of Health) (*see* **Note 8**).
3. Image-Pro Plus (Media Cybernetics).
4. Pipeline Pilot (Accelrys; San Diego, CA).
5. A terabyte server (Sentinel Small Office Storage Server, Amazon) (*see* **Note 9**).

2.6 Data Analysis

1. The R Project for Statistical Computing (http://www.r-project.org/, R Development Core Team).

3 Methods

3.1 Fluorescently Tagged Proteins

3.1.1 N-Terminal Fragment of htt Fused to the N-Terminus of a Fluorescent Protein

1. Isolate the plasmid DNA encoding GFP fused to WT or mutant htt (the exon 1 fragment or longer) with a plasmid purification kit (*see* **Notes 1** and **2**). Follow the manufacturer's instructions.
2. Adjust concentration to 0.5–1.5 μg/ml with water.
3. Store the plasmid at 4 °C for up to 6 months.

3.1.2 A Morphology and Viability Fluorescent Marker

1. Isolate the plasmid DNA encoding a red morphology and viability marker (such as mRFP or mCherry) with a plasmid purification kit (*see* **Notes 3** and **4**); follow manufacturer's instructions.

2. Adjust concentration to 0.5–1.5 μg/ml with water.
3. Store the plasmid at 4 °C for up to 6 months.

3.2 Preparation of Neuronal Cultures

1. One day before preparing the cultures, prepare the plates. Into 100 ml of sterile water, add 5 ml of poly-D-lysine solution and a half vial of mouse laminin (the remainder can be kept at −80 °C for later use). Mix well.
2. *To a 96-well plate*: add 150 μl of the coating mix (poly-D-lysine/laminin solution). *To a 24-well plate*: add 500 μl of the coating mix (*see* **Note 5**). Swirl the plates to ensure that the coating mix completely covers the bottom of the wells.
3. Leave the plates in a 37 °C/5 % CO_2 incubator overnight.
4. Wash the plates twice with sterile water (150 μl of water for a 96-well plate and 500 μl for a 24-well plate). Remove the final wash and leave the plates in a 37 °C/5 % CO_2 incubator.
5. Make neuronal growth medium: mix neurobasal medium with B27 vitamin supplement (50× stock), GlutaMAX (100× stock) (catalog number 35050, GIBCO), and penicillin/streptomycin (100× stock) to a 1× final concentration. Keep in a 37 °C water bath.
6. Make Opti-MEM-glucose (4 ml of 2.5 M glucose per 500 ml of Opti-MEM). Keep in a 37 °C water bath.
7. Prepare DM/KY solution (300–500 ml): dilute the 10× KY stock into an appropriate volume of DM. Keep on ice.
8. Prepare the trypsin inhibitor solution: add 150 mg of trypsin inhibitor to 10 ml of DM/KY. The solution will become yellow. Adjust the pH of the solution with 1 M NaOH until it is pink again (pH 7.5). Keep at room temperature.
9. Prepare the solution for papain: add 2–3 mg of L-cysteine to 10 ml of DM/KY. Adjust pH of the solution with 5 M NaOH until it is pink again (pH 7.5). Keep at room temperature.
10. Pour ice-cold DM/KY solution into two 10-cm culture dishes (one for the pup heads and one for the brains) and into one 6-cm dish (for the dissected striatum). Keep dishes on ice.
11. Sterilize the dissection tools with 70 % (v/v) ethanol.
12. Sacrifice a timed-pregnant rat (or a mouse) according to an animal protocol approved at your institution (*see* **Note 10**).
13. After an animal is sacrificed, clean the belly with 96 % (v/v) alcohol. Cut along the abdomen and remove the uterus. Place the pups into the large culture dish.
14. Cut off the pup heads with scissors and put them in a 10-cm dish with DM/KY on ice.
15. Under a dissection microscope, remove the skin from a skull. Hold the head with forceps through the eyes. Use the other

forceps to incise the skin towards the eyes and peel the skin and open the skull. Cut the optic nerves. Take the chemical spatula, dig underneath the brain, and scoop it out. Place the brain into a new 10-cm dish with DM/KY on ice.

16. Repeat the process with other heads.
17. Dissect the striatum. Orient yourself so that the brain is facing forward. For each hemisphere, use your forceps to dissect longitudinally down the hemisphere. Your goal is to expose the structures just underneath the superficial cortex. Pierce the ventral surface of the cortex of each hemisphere to access the lateral ventricle. The capillary network and the choroid plexus should be visible. At this developmental stage, the striatum is the structure of brain tissue bulging into the lateral ventricle from the midline. The lateral edge of the striatum forms a semicircle. Isolate the striatum and discard the remaining brain tissue (mostly cortex and hippocampus). Dissect away the remaining cortex from the striatum. Dissect the striatum and place it in a new 10-cm dish with DM/KY on ice (*see* **Note 11**).
18. Repeat the process with the other cortical hemisphere and other brains. Keep the striata all together in DM/KY on ice.
19. Prepare the papain solution: add 100 U of papain to the cysteine/DM/KY solution.
20. Filter the trypsin inhibitor solution and papain solution through a 0.20-μm filter and 30-ml syringe. Place both the trypsin inhibitor solution and the papain solution in the 37 °C water bath.
21. Clean up after the dissection (5 min).
22. Transfer the striata with a cut 500-μl tip by pipettor suction to a 15-ml conical tube. Let the tissue settle and remove the extra DM/KY solution.
23. Add 10 ml of warm papain solution to the striata and incubate at 37 °C for 10 min. Carefully swirl the tube after 5 min.
24. Carefully remove the papain solution.
25. Add warm trypsin inhibitor solution and incubate at 37 °C for 10 min. Carefully swirl the tube after 5 min.
26. Remove the trypsin inhibitor solution and wash the striata with 10 ml of warm Opti-MEM-glucose. Remove the Opti-MEM-glucose solution.
27. Under a sterile hood, add 5 ml of Opti-MEM-glucose. Triturate gently several times with a 5-ml pipette until the solution turns cloudy.
28. Allow the tissue to settle. Take the supernatant and transfer it to a 50-ml conical tube. Keep it under the sterile hood at room temperature.

29. Add 5 ml of new Opti-MEM-glucose to the striata and repeat trituration. Triturate 8–10 times for striatum collected from 10 to 15 rat brains or 5 times for striatum collected from 5 to 6 mouse brains.
30. Allow the debris to settle in the 50-ml conical tube. Take a 5-ml pipette and remove the debris.
31. Counting neurons: mix the neuron suspension in the 50-ml conical tube. Take a 10-µl aliquot and add it to a tube that contains 10 µl of Opti-MEM-glucose and 10 µl of trypan blue. Carefully mix and add 10 µl to the hemocytometer. Count the cells in the 16-box squares in the two opposite corners of the field. Average the two counts and multiply the average by 30,000 to get the number of cells per ml.
32. Plate cells to a final concentration of 100,000 per well of a 96-well plate (in 100–200 µl of plating Opti-MEM-glucose solution) or 0.6–0.75 million per well of a 24-well plate (in 500–1,500 µl of plating Opti-MEM-glucose solution). Dilute the cells with Opti-MEM-glucose solution before plating, if needed. Swirl the plate to make sure cells are evenly distributed.
33. Incubate the plates at 37 °C for 1 h.
34. Check the cells under the microscope to ensure that the neurons adhered to the well surface.
35. Replace the Opti-MEM-glucose solution with warm neurobasal medium (that contains B27 vitamin supplement, GlutaMAX, and antibiotics): 200 µl of neurobasal medium per well of a 96-well plate, 1 ml of neurobasal medium per well of a 24-well plate.

3.3 Transfection

1. Prepare neurobasal/KY solution: dilute the 10× KY stock into an appropriate volume of neurobasal medium. Keep it in the 37 °C water bath.
2. Warm Opti-MEM to room temperature.
3. For each transfection sample, prepare the DNA/Lipofectamine 2000 complexes according to the manufacturer's protocol (*see* **Note 12**). Keep the tubes at room temperature for 20 min to allow the DNA/Lipofectamine 2000 complexes to form.
4. Use 5 days in vitro (DIV) neuronal cultures for transfection.
5. Wash neuronal cultures twice with neurobasal/KY solution.
6. Add 150 µl of neurobasal/KY solution per well of a 96-well plate or 500 µl of neurobasal/KY solution per well of a 24-well plate.
7. Vortex the DNA/Lipofectamine 2000 complexes, add them to neuronal cultures (*see* **Note 12**), and swirl the plate.

8. Incubate the plates in the 37 °C/5 % CO_2 incubator for 0.5–2.5 h (*see* **Note 13**).
9. Wash neuronal cultures twice with neurobasal medium.
10. Add 200 µl of neurobasal medium per well of a 96-well plate or 1 ml of neurobasal medium per well of a 24-well plate.

3.4 Longitudinal Single-Cell Image Acquisition

Several commercially available systems are capable of performing automated image acquisition and some forms of automated image analysis [18]. High-content screening (HCS) systems, such as Opera (PerkinElmer) or IN Cell Analyzer (GE Healthcare), provide fast image acquisition and powerful data-processing capabilities. In general, these systems tend to be oriented to the analysis of snapshots of immunocytochemically stained, fixed cells rather than live-cell imaging, and their cost and the extent in which their proprietary algorithms allow for customization of each user's applications vary. However, the main difference between the commercial systems and those we described above is the ability to do longitudinal single-cell analysis over arbitrarily long periods of time. This feature allows our system to unravel complex cause-and-effect relationships and to detect the effects of manipulations with extraordinary sensitivity. For a more in-depth overview of automated image acquisition platforms with primary neurons, *see* ref. 19.

Although we have automated image acquisition to improve precision and throughput, we can generate longitudinal series of images of single cells and extract datasets that are amenable to analysis with powerful statistical tools described below. Here we present a general protocol to generate longitudinal images of single cells spanning arbitrary time intervals. The four main steps are registration, stage movement, focus, and acquisition:

1. *Registration*. In most of our experiments, cultured cells are returned to an incubator between imaging intervals, so many experiments can be run on the same microscope in parallel. To find the same neuron each time the plate is returned to the stage, a method to register the position of the plate on the microscope is critical. Most manufacturers stamp alphanumeric codes on the plate itself, a fiduciary mark that can be used to register the plate position. If the plate lacks such a mark, the user can make one with a marker or by etching the plastic. At the first time point, an image of the fiduciary mark on the plate is collected and stored as a reference image. Subsequently, each time the same plate is imaged, the fiduciary mark on the plate is aligned with the reference image. Alignment can be performed manually.
2. *Stage movements*. To begin image acquisition, the plate needs to be moved from the fiduciary mark to a well of interest.

This can be accomplished by using the computer to direct the automated stage to a specific *x*–*y* location. We typically begin with the center of the well located at the most far-left position in the top row of the plate. In cases where multiple fields from the same well are desired, the user must systematically collect images of adjacent microscope fields. We use the computer to instruct the stage to make a pattern of movements relative to the fiduciary mark. This can also be done manually by creating an ordered list of coordinates visited on the first time point and then controlling the automated stage to return to each coordinate on that list during subsequent time points. More conveniently, some acquisition programs provide built-in functionality for moving between wells of a standard microplate and for imaging an array within a well. We found that a 3×3 image array using a $20\times$ objective often contains enough cells to powerfully measure relationships between expression levels, IB formation, neuronal morphology, and survival while maintaining high throughput. To ensure that the array of images from a single well have optimal image content, the physical dimensions of a microscope field should be determined and used to program the stage to collect images from contiguous but slightly overlapping fields. This can be done using a reference slide with grids of known distance to determine the physical dimensions of a pixel.

3. *Focus*. Accurate and consistent focus is a critical issue for measuring fluorescence-intensity levels and subcellular changes such as inclusion formation. This can be done manually using a brightfield image before fluorescence imaging, but it is tedious and reduces throughput. To increase throughput, we have used automated focusing algorithms that are image-based or based on the direct detection of the physical distance between the objective and the bottom of the plate. Although the image-based algorithms were often very good, the physical methods have proven to be more accurate, faster, and especially well suited to plates that contain ≥96 wells.
4. *Acquisition*. Acquisition of fluorescence images can be done manually or with an automated acquisition program, which should have functions for controlling the excitation and emission filters, the polychroic cube, and the exposure time. To limit bleed-through of fluorescence from one channel to another, we use fluorescent proteins whose emissions are relatively well separated with commercially available optical filters. A common choice is cyan, yellow, and red fluorescent proteins for imaging morphology or when creating reporter constructs. The length of illumination required to generate a quality image will depend significantly on the expression level and quantum efficiency of the fluorescent protein, the efficiency of

the optical path, and the sensitivity of the camera. With a standard CCD camera, exposure times from 100 ms to 1 s provide a sufficient balance between signal collection and throughput (*see* **Note 14**) although much lower exposure times are possible with EM-CCD cameras.

3.5 Image Analysis and Storage

We use survival analysis, a statistical tool, to quantify how the factors that were measured during the course of the experiment contribute to a fate that is being measured [11]. Despite its name, survival analysis is not limited to the study of survival, but in fact can be used with our system to study any endpoint that can be measured over time from collected images.

For these analyses, the survival time is measured for each neuron from the moment a transfected neuron is visualized until its death, indicated by the abrupt disappearance of the transfected marker. Survival time for each neuron in a cohort is tabulated, and a survival curve for the neuronal cohort is constructed with software (R or StatView). Neurons that survived the entire experiment are weighted differently to account for an indeterminate survival time. Survival functions are fit with Kaplan–Meier analysis, and differences between the cohorts are assessed with the log-rank test. The cumulative nature of the analysis makes it much more sensitive (100–1,000×) than approaches offered by commercial image analysis software, which depend on averaged responses measured at particular time points (*see* ref. 3).

A hazard function, which describes the instantaneous risk that a member of the cohort will reach the endpoint of interest, can be obtained from the survival function (StatView or R). This analysis can be useful for assessing whether a change of interest in the cells we are following is associated with an increased or decreased likelihood that the cohort will achieve the endpoint of interest. In simple terms, as it applies to neurodegeneration, this analysis helps us determine whether an intermediate change is likely to be incidental, part of the pathogenic process, or part of a coping response.

If two cohorts are being compared and the differences in hazard between the cohorts are proportional over the course of the study, the data can be analyzed further using a CPH analysis. CPH analysis makes it possible to quantify the contribution, if any, of specific factors or covariates to a given cell's fate. With CPH analysis, increasingly accurate quantitative multivariate models can be constructed that predict outcomes in terms of a series of measurable covariates. CPH analysis deduces a coefficient for each covariate whose magnitude and sign indicate its importance and whether that covariate increases or decreases the likelihood of a particular fate.

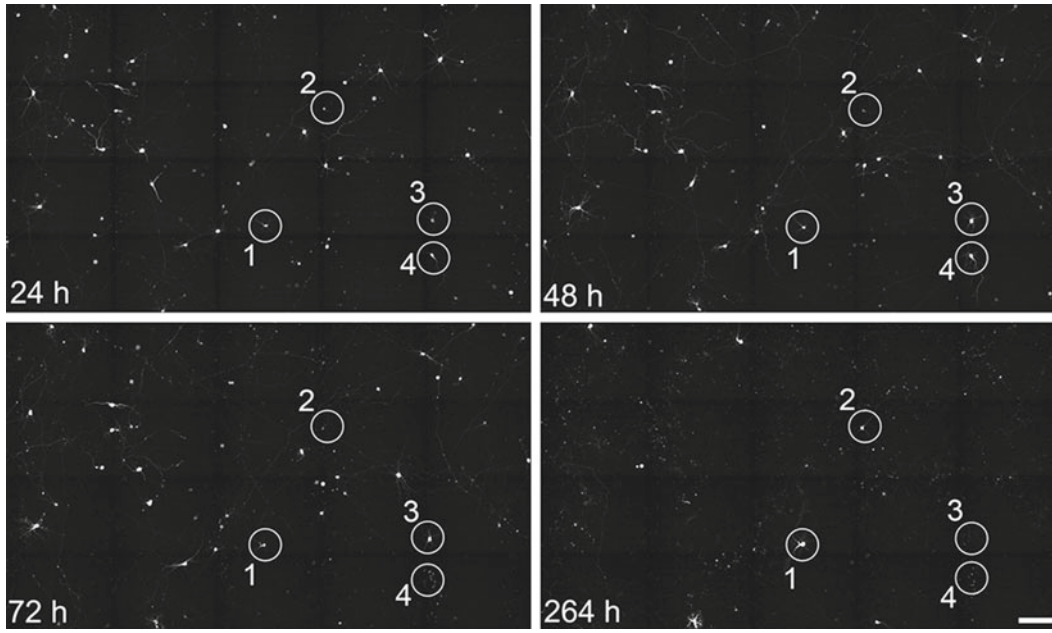

Fig. 1 Images collected at arbitrary intervals (i.e., 24, 48, 72, and 246 h after transfection) demonstrate the ability to return to the same field of neurons and track them over time. Every image is a montage of 20 nonoverlapping images captured in one well of a 96-well plate. Neurons express mCherry and can be identified using a custom-made algorithm (as an example, four neurons are circled and tracked). Neurons #1 and 2 survived throughout the experiment, neuron #3 died between 72 and 264 h, and neuron #4 died between 48 and 72 h. Images collected with a 20× objective. Scale bar is 300 μm

Below, we present a general protocol that might be used for analyzing images:

1. *Image organization*. Depending on the precision of the stage alignment, cells at the edge of a microscope field can appear in one image but also in a subsequent one. To avoid losing data at the edge of images and to facilitate the analysis of structures that can span multiple fields (e.g., axons, dendrites), we begin image analysis by electronically stitching images of all the microscope fields from the same well into a montage. Many image analysis programs offer this function, but it can also be performed manually. The key is to collect images of contiguous microscope fields that overlap slightly so as to ensure accurate alignment. One can then create a montage of the stitched images from one well at each time point and then combine those montages into a single image "stack" in which the *z*-axis represents time (Fig. 1). Since small errors occur during registration and stage movement, use of an alignment algorithm will aid in later analysis (*see* **Note 15**).
2. *Image segmentation*. This next step of the analysis is the most important and also the most difficult. First, we choose a threshold

intensity and identify pixels that exceed this threshold to consider for further analysis. The second step is a filter that analyzes contiguous groups of pixels to determine if the size of the group and the pattern of intensities within the border fit within our predetermined criteria for an object that we count as a neuronal soma. This is critical for distinguishing between positive pixels that belong to genuine cellular objects of interest versus those that represent debris, noise, or parts of cells. The algorithm that we developed performs with 80–90 % accuracy. Commercial image analysis programs often contain thresholding and spatial filter functions, which can be adapted for this purpose. For a more in-depth overview of image segmentation, *see* ref. 19 (Image Segmentation).

3. *Longitudinal tracking.* To get the benefits of longitudinal analysis, individual neurons must be tracked over the course of the experiment. Once image analysis has been performed on the first montage of a series for a particular experiment, each cell that has been identified is assigned a unique identifying number. The precise *x*–*y* location is recorded and used in images collected at subsequent time points to find the same cell or to determine that it has died and disappeared during the interval. As long as the movement of cells between images is relatively small and the "positive" cells are mostly well separated from each other, automated tracking is often possible. Some commercially available automated tracking programs do a reasonable job; alternatively, tracking can be performed manually.
4. *Analysis of image features.* Once a neuronal feature to analyze is selected (e.g., expression levels, IB formation, neurite length, or neurite branching), depending on the neuronal feature selected, open-source or commercially available software might exist with the functionality (or extensibility) to extract the desired information. If not, this may be done with manual intervention (*see* **Note 8**). Fluorescence data from the same cell in other channels can also be extracted. We binarize images of the cells generated from the fluorescence of the morphology marker and multiply those by the images of the same cell from the other fluorescence channels. The extracted information is then quantified and linked to that cell's unique identifier number.
5. *Survival analysis.* To perform survival analysis, a measureable endpoint must be chosen, and the time point when that endpoint is manifest must be determined. For survival analysis, the algorithm we developed to track neurons over time makes a determination of the time point at which death has occurred (*see* **Note 16**). Survival datasets are used to construct the

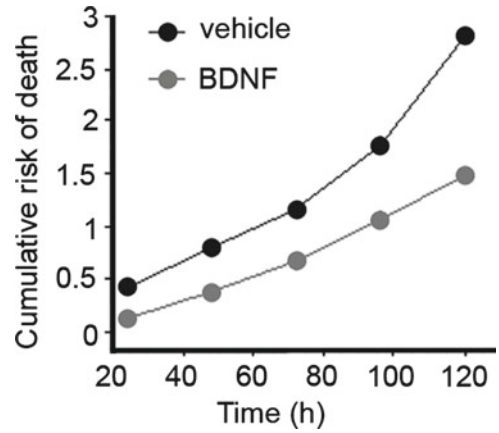

Fig. 2 An example of survival analysis. Striatal neurons transfected with mCherry and $Htt^{ex1}{}_{72Q}$-GFP were treated with 100 ng/ml BDNF or vehicle and followed with an automated microscope. Cumulative risk-of-death statistics were calculated from Kaplan–Meier curves. BDNF reduced the risk of death (i.e., improved survival) of neurons. * $p < 0.001$ (Mantel-Cox test)

survival curves (*see* **Notes 17** and **18**). Kaplan–Meier curves are used to estimate survival and hazard functions with R or StatView. Differences in Kaplan–Meier curves (e.g., differences between survival of different neuronal populations) are assessed with the log-rank test (Fig. 2).

6. *Cox proportional hazard analysis.* If intermediate measures were made of putative covariates (e.g., IB formation, expression levels), their contribution to fate can be estimated with CPH analysis. These types of analyses can be performed with commercially available or open-source programs (StatView or R).

4 Notes

1. We routinely use the exon 1 fragment of WT and mutant (containing either normal (Q_{17}) or disease-associated (Q_{47}, Q_{72}, Q_{103}) polyQ expansions) htt and longer N-terminal portions of htt (171, 480, 586 amino acids) [2–4, 14–16]. This approach to in vitro disease modeling can be applied broadly. In our lab, we developed a model of familial amyotrophic lateral sclerosis, based on expression of a fluorescently tagged version of the protein TDP-43 in cultured cortical neurons [20], and two models of Parkinson disease, based on the expression of

fluorescently tagged α-synuclein [21] and LRRK2 (personal communication, Steven Finkbeiner, Gaia Skibinski).

2. It is very important to use a truly monomeric version of a fluorescent protein, because dimerization or tetramerization can greatly affect the biochemistry of the protein to which it is fused. In our lab, we use a wide variety of monomeric fluorescent proteins [2–4, 14–16]. We prefer fluorescent proteins that have a high quantum yield and resist photobleaching. These characteristics allow us to use minimal illumination and avoid unwanted phototoxicity, and they simplify the analysis. Examples of fluorophore triads that can be resolved with most filter-based epifluorescence systems include monomeric (m) Apple or mCherry (red channel), Venus or mCitrine (yellow channel), and CFP or Cerulean (cyan channel).
3. Mutant htt forms IBs, which sequester diffuse mutant htt. After an IB has formed, it is difficult to accurately determine neuronal morphology using the fluorescence of mutant htt molecules. Therefore, to measure morphology and viability, it is important to use an inert fluorophore that is physically separate from the fluorophore fused to htt.
4. We routinely use mApple or mCherry (both are red fluorescent proteins) as a morphology and viability marker [3, 4]. Any red fluorescent protein can be used in a combination with htt fused to a yellow (mCitrine) or green (EGFP) fluorescent protein. Alternatively, htt could be labeled red and a morphology marker can be green.
5. The choice of plate type is based on several factors. 24-well plates (Corning) are cheaper and may work well for pilot experiments but allow for fewer conditions on one plate. In addition, each well requires more reagents (e.g., plasmids, transfection reagent, media, drugs). In our lab, we routinely use the Swiss TPP 96-well plates.
6. Ca^{2+} phosphate-based and lipid reagent-based (e.g., Lipofectamine 2000) methods can work comparably in the hands of an experienced user. The Ca^{2+}-phosphate method is very cheap but requires the detection of a Ca^{2+}-phosphate/DNA precipitate with a microscope, making this method less reproducible. Lipofectamine 2000 is expensive but gives more reproducible transfection, amenable to automated transfection, and easier for novices to perform. Other means of DNA delivery (e.g., viral delivery and electroporation, including nucleofection) produce a very high transfection efficiency, which leads to many transfected neurons with overlapping dendrites. This can make it difficult to identify the same individual neurons in a sequence of images.

7. Several commercial systems for image acquisition are now available, including Opera, Operetta, and UltraView (PerkinElmer); IN Cell Analyzer (GE Healthcare); IC200 (Vala Lifesciences); ImageXpress Micro, Ultra, and Velos (Molecular Devices); Cellomics ArrayScan (Thermo Scientific); Pathway 435 and 855 (BD); and Scan^R (Olympus) [18].
8. ImageJ was designed with open-source software and a variety of Java plugins. Some algorithms can be downloaded from the ImageJ website:

   http://rsb.info.nih.gov/ij/plugins/

   For additional reading, *see* ref. 22.

   An algorithm for ImageJ, NeuriteTracer, described in the following reference, measures neurite length and neuronal cell numbers in neuronal cultures:

   http://www.ncbi.nlm.nih.gov/pubmed/17936365

   Another algorithm for neurite tracing and quantification is described here:

   http://www.imagescience.org/meijering/software/neuronj/
9. For our typical scan of a 96-well plate, we collect images of nine microscope fields with fluorescence from two channels (a morphology/viability red fluorescent marker and green fluorescent protein-fused htt). This results in a collection of 18 images per well and requires 20 GB of storage space (image file size from a megapixel charged-coupled device (CCD) with 12–16 bit depth can be on the order of megabytes).
10. We prefer embryonic stage (E) 17 for rats for the striatal cultures, because the striatum is fairly well developed at this stage but much easier to dissect than at later gestational stages when the cortex is more fully developed. We also prefer rat E17 for isolating the cortex in comparative experiments (striatal cultures vs. cortical neurons), but E19–21 or even postnatal day 0 pups can be used, which will yield more neurons. For mouse cultures, we culture neurons from embryos at 18–20 days of gestation.
11. The striatum can also be isolated using coronal dissection. For a video *see* ref. 23.
12. Invitrogen's protocol can be found here:

    http://tools.invitrogen.com/content/sfs/manuals/lipofectamine2000_man.pdf

    We start any new transfection by testing the recommended concentrations of Lipofectamine 2000 reagent and the ratios of the transfected plasmids. The usual ratio is 2:1 for htt-GFP:mRFP.

13. Although the protocol suggests that "it is not necessary to remove complexes or change/add medium after transfection," we always remove complexes from neuronal cultures after 0.5–2.5 h. Longer incubations result in significant toxicity.
14. Transfected neurons can be imaged as early as 2 h after transfection. For imaging HD-model cells, we typically start observing neurons 12–24 h post-transfection and monitor them once daily for 14 days. Our longest experiment went 6 months. If an imaging system is not equipped with a controlled-environment chamber, use a strip of parafilm to seal the plate and limit the length of time the plate is outside the incubator.
15. Small errors occur during registration and stage movement; therefore, there is a portion of each field that might be missing from one image or another. Since we can only follow neurons that are in all the images, to avoid discarding the data, we montage the adjacent images. We use the Stitching 2D/3D plugin for ImageJ to montage our images [24]. For image alignment we use MultiStackReg, an adaption of StackReg [25].
16. We use a custom-made algorithm that identifies neuronal somata in a montaged image of microscope fields, tracks them from images collected at subsequent time points, and detects when an individual neuron died (Fig. 1). This custom algorithm records the tabulated survival times for each neuron in an Excel file along with information about fluorescence intensity and neuron morphology at each time point that it is alive.
17. To quantify neuronal survival, we tabulate survival time for each neuron in a cohort, and a survival curve for this cohort is constructed with StatView software. Neurons surviving the entire experiment are weighted differently (i.e., censored) to show that a precise survival time was not determined [3, 4].
18. For statistical analyses, we have adopted the convention of defining survival time as the imaging time point at which a neuron is last seen alive.

Acknowledgments

This work was supported by R01 2NS039746 and 2R01 NS045191 from the National Institute of Neurological Disease and Stroke, P01 2AG022074 from the National Institute on Aging, and the Gladstone Institutes (S.F.), the Milton Wexler Award, and a fellowship from the Hereditary Disease Foundation (A.T.). Gladstone Institutes received support from a National Center for Research Resources Grant RR18928-01. Kelley Nelson provided administrative assistance, and Gary C. Howard and Anna Lisa Lucido edited the manuscript.

References

1. Saudou F, Finkbeiner S, Devys D, Greenberg ME (1998) Huntingtin acts in the nucleus to induce apoptosis but death does not correlate with the formation of intranuclear inclusions. Cell 95:55–66
2. Miller J, Arrasate M, Shaby BA, Mitra S, Masliah E, Finkbeiner S (2010) Quantitative relationships between huntingtin levels, polyglutamine length, inclusion body formation, and neuronal death provide novel insight into huntington's disease molecular pathogenesis. J Neurosci 30:10541–10550
3. Arrasate M, Finkbeiner S (2005) Automated microscope system for determining factors that predict neuronal fate. Proc Natl Acad Sci USA 102:3840–3845
4. Tsvetkov AS, Miller J, Arrasate M, Wong JS, Pleiss MA, Finkbeiner S (2010) A small-molecule scaffold induces autophagy in primary neurons and protects against toxicity in a Huntington disease model. Proc Natl Acad Sci USA 107:16982–16987
5. Consortium, H. D. i (2012) Induced pluripotent stem cells from patients with Huntington's disease show CAG-repeat-expansion-associated phenotypes. Cell Stem Cell 11:264–278
6. Gutekunst CA, Li SH, Yi H, Mulroy JS, Kuemmerle S, Jones R, Rye D, Ferrante RJ, Hersch SM, Li XJ (1999) Nuclear and neuropil aggregates in Huntington's disease: relationship to neuropathology. J Neurosci 19:2522–2534
7. Schilling G, Savonenko AV, Klevytska A, Morton JL, Tucker SM, Poirier M, Gale A, Chan N, Gonzales V, Slunt HH, Coonfield ML, Jenkins NA, Copeland NG, Ross CA, Borchelt DR (2004) Nuclear-targeting of mutant huntingtin fragments produces Huntington's disease-like phenotypes in transgenic mice. Hum Mol Genet 13:1599–1610
8. Benn CL, Landles C, Li H, Strand AD, Woodman B, Sathasivam K, Li SH, Ghazi-Noori S, Hockly E, Faruque SM, Cha JH, Sharpe PT, Olson JM, Li XJ, Bates GP (2005) Contribution of nuclear and extranuclear polyQ to neurological phenotypes in mouse models of Huntington's disease. Hum Mol Genet 14: 3065–3078
9. Zala D, Bensadoun JC, Pereira de Almeida L, Leavitt BR, Gutekunst CA, Aebischer P, Hayden MR, Deglon N (2004) Long-term lentiviral-mediated expression of ciliary neurotrophic factor in the striatum of Huntington's disease transgenic mice. Exp Neurol 185:26–35
10. Kuemmerle S, Gutekunst CA, Klein AM, Li XJ, Li SH, Beal MF, Hersch SM, Ferrante RJ (1999) Huntington aggregates may not predict neuronal death in Huntington's disease. Ann Neurol 46:842–849
11. Slow EJ, Graham RK, Osmand AP, Devon RS, Lu G, Deng Y, Pearson J, Vaid K, Bissada N, Wetzel R, Leavitt BR, Hayden MR (2005) Absence of behavioral abnormalities and neurodegeneration in vivo despite widespread neuronal huntingtin inclusions. Proc Natl Acad Sci USA 102:11402–11407
12. Warby SC, Chan EY, Metzler M, Gan L, Singaraja RR, Crocker SF, Robertson HA, Hayden MR (2005) Huntingtin phosphorylation on serine 421 is significantly reduced in the striatum and by polyglutamine expansion in vivo. Hum Mol Genet 14:1569–1577
13. Graham RK, Slow EJ, Deng Y, Bissada N, Lu G, Pearson J, Shehadeh J, Leavitt BR, Raymond LA, Hayden MR (2006) Levels of mutant huntingtin influence the phenotypic severity of Huntington disease in YAC128 mouse models. Neurobiol Dis 21:444–455
14. Arrasate M, Mitra S, Schweitzer ES, Segal MR, Finkbeiner S (2004) Inclusion body formation reduces levels of mutant huntingtin and the risk of neuronal death. Nature 431:805–810
15. Mitra S, Tsvetkov AS, Finkbeiner S (2009) Single neuron ubiquitin-proteasome dynamics accompanying inclusion body formation in huntington disease. J Biol Chem 284: 4398–4403
16. Miller J, Arrasate M, Brooks E, Libeu CP, Legleiter J, Hatters D, Curtis J, Cheung K, Krishnan P, Mitra S, Widjaja K, Shaby BA, Lotz GP, Newhouse Y, Mitchell EJ, Osmand A, Gray M, Thulasiramin V, Saudou F, Segal M, Yang XW, Masliah E, Thompson LM, Muchowski PJ, Weisgraber KH, Finkbeiner S (2011) Identifying polyglutamine protein species in situ that best predict neurodegeneration. Nat Chem Biol 7:925–934
17. Ortega Z, Diaz-Hernandez M, Maynard CJ, Hernandez F, Dantuma NP, Lucas JJ (2010) Acute polyglutamine expression in inducible mouse model unravels ubiquitin/proteasome system impairment and permanent recovery attributable to aggregate formation. J Neurosci 30:3675–3688
18. Lang P, Yeow K, Nichols A, Scheer A (2006) Cellular imaging in drug discovery. Nat Rev Drug Discov 5:343–356
19. Sharma P, Ando DM, Daub A, Kaye JA, Finkbeiner S (2012) High-throughput screening in primary neurons. Methods Enzymol 506:331–360

20. Barmada SJ, Skibinski G, Korb E, Rao EJ, Wu JY, Finkbeiner S (2010) Cytoplasmic mislocalization of TDP-43 is toxic to neurons and enhanced by a mutation associated with familial amyotrophic lateral sclerosis. J Neurosci 30: 639–649
21. Nakamura K, Nemani VM, Azarbal F, Skibinski G, Levy JM, Egami K, Munishkina L, Zhang J, Gardner B, Wakabayashi J, Sesaki H, Cheng Y, Finkbeiner S, Nussbaum RL, Masliah E, Edwards RH (2011) Direct membrane association drives mitochondrial fission by the Parkinson disease-associated protein alpha-synuclein. J Biol Chem 286:20710–20726
22. Glory E, Murphy RF (2007) Automated subcellular location determination and high-throughput microscopy. Dev Cell 12:7–16
23. Chiu K, Lau WM, Lau HT, So KF, Chang RCC (2007) Micro-dissection of rat brain for RNA or protein extraction from specific brain region. J Vis Exp (7):e269. doi: 10.3791/269
24. Preibisch S, Saalfeld S, Tomancak P (2009) Globally optimal stitching of tiled 3D microscopic image acquisitions. Bioinformatics 25: 1463–1465
25. Thevenaz P, Ruttimann UE, Unser M (1998) A pyramid approach to subpixel registration based on intensity. IEEE Trans Image Process 7:27–41